doi: 10.18323/2782-4039-2023-2-64-8

Cyclic regularities of the acoustic emission generation during plasma-electrolytic oxidation of an Al–Mg alloy in the bipolar mode

Igor A. Rastegaev*[1], PhD (Physics and Mathematics),
senior researcher of the Research Institute of Advanced Technologies
Marat R. Shafeev[2], junior researcher of the Research Institute of Advanced Technologies
Inna I. Rastegaeva[3], senior lecturer of Chair "Nanotechnologies, Materials Science and Mechanics"
Anton V. Polunin[4], PhD (Engineering), leading researcher of the Research Institute of Advanced Technologies
Mikhail M. Krishtal[5], Doctor of Sciences (Physics and Mathematics), Professor,
chief researcher of the Research Institute of Advanced Technologies
Togliatti State University, Togliatti (Russia)

***E-mail: RastIgAev@yandex.ru, I.Rastegaev@tltsu.ru**

[1]ORCID: https://orcid.org/0000-0003-3807-8105
[2]ORCID: https://orcid.org/0000-0002-4490-6547
[3]ORCID: https://orcid.org/0000-0002-7634-2328
[4]ORCID: https://orcid.org/0000-0001-8484-2456
[5]ORCID: https://orcid.org/0000-0001-7189-0002

Received 03.05.2023 *Accepted 13.06.2023*

Abstract: The paper analyzes the features of the acoustic emission (AE) signal generation during plasma-electrolytic oxidation (PEO) of the AMg6 aluminum alloy in a bipolar (anode-cathode) pulsed mode within each cycle of voltage application. The authors studied the range of PEO modes that almost completely covers all standard technological modes for processing aluminum alloys by the current densities (6–18 A/dm^2) and current ratio in half-cycles (0.7–1.3), which allowed fixing and studying the AE accompanying the formation of oxide layers for various purposes. For the first time, due to AE registration, a new PEO stage was identified, in which there was no microarc breakdown to the substrate, but which was accompanied by an increase in the layer thickness, and the nature of which has not yet been determined. According to the known features of the oxidation stages, the authors systematized the repetitive forms of AE manifestation in the cycles of exposure and identified their five types and three subtypes. The study shows that the approach used to establish the PEO stages by the "acoustic emission amplitude" parameter has poor accuracy, since it does not take into account the form of signals and the half-period of their registration. Therefore, the authors developed and tested a new approach for analyzing AE frames synchronously with the cycles of change in the forming voltage during PEO, and proposed a new "acoustic-emission median" parameter, which allows identifying the main types and subtypes of signals accompanying the oxidation stages. An experimental study of the proposed AE parameter was carried out to identify these PEO stages, which confirmed the operability, high accuracy and sensitivity of the proposed parameter to the subtypes of AE signals recorded at the cathode stage of "soft sparking". The latter is of particular interest, since it is a means of studying a given oxidation stage with a resolution equal to the exposure cycle.

Keywords: aluminum alloy; plasma electrolytic oxidation; acoustic emission; microarc discharges.
Acknowledgments: This work was supported by the Russian Science Foundation (Project No. 20-79-10262, https://rscf.ru/project/20-79-10262/).
For citation: Rastegaev I.A., Shafeev M.R., Rastegaeva I.I., Polunin A.V., Krishtal M.M. Cyclic regularities of the acoustic emission generation during plasma-electrolytic oxidation of an Al–Mg alloy in the bipolar mode. *Frontier Materials & Technologies*, 2023, no. 2. DOI: 10.18323/2782-4039-2023-2-64-8.

INTRODUCTION

Today, one of the relevant issues of the technology of plasma electrolytic, or microarc, oxidation (PEO or MAO) of the surface of products made of valve group metals (Al, Mg, Ti, Zr, Nb, etc.) is to monitor the process of formation of a multifunctional oxide "coating" (oxide layer). According to [1], the multifunctionality of coatings is the possibility of their application in various fields of science, and technology under conditions that differ vastly in the main damaging factors (mechanical-chemical, chemical-thermal, mechanical-electrical, etc.). It is known [2] that the ability to resist the impact of external and internal damaging factors is provided by the physicochemical properties of oxide layers (adhesion, hardness, wear resistance, etc.), which, in turn, are determined by a complex of characteristics and factors – structural (thickness, porosity, residual strains, etc.), phase (qualitative and quantitative composition), morphology of the layer, and its defectiveness [2]. Many authors show that the uniformity of the properties of oxide layers in thickness (sublayers) depends on the PEO process parameters, more specifically, the frequency of forming pulses and current density [3], the presence of the cathode current component [4; 5], and its power ratio with the anode component [6], electrolyte composition [7] and its quality [8], which together determine the types of formed discharges and their power [9]. In particular, it was established in [3], that the application of the increased current densities (70–90 A/dm^2) in combination with high frequencies of forming pulses (up to 900 Hz) leads to a decrease in the porosity and non-uniformity of oxide layers, due to a decrease in the surface density of microdischarges. In [4; 5]

the authors found that an increase in the cathode component during PEO of an aluminum alloy, and a transition to the "soft sparking" mode can lead to the occurrence of developed nanosized porosity in combination with a barrier layer densification at the "metal substrate – oxide layer" interface [4], which is also observed during the magnesium alloy PEO [6]. In [5], it was found that the cathode half-cycle (negative polarization) during the PEO of aluminum alloy leads to additional formation of aluminum hydroxide, with a decrease in the resistance to microarc breakdown of the barrier layer followed by the formation of stable Al_2O_3 modifications, as a result of $Al(OH)_3$ dehydration in the anode half-cycle, and to the barrier layer densification, which ultimately improves the uniformity and protective properties of the oxide layers. Therefore, the possibility of the PEO process in situ monitoring, recognition of its stage, microarc breakdown type, and the emerging microarc discharge (MAD) allows establishing the mechanism of surface oxidation and oxide layer formation at a time, and thus, at the stage of developing PEO modes, organizing feedback to control the energy released in the MAD breakdown channels directly in the oxidation process, i.e., controlling the quality and functional properties of the oxide layers.

Nowadays, several methods for PEO process monitoring have been proposed and tested already. They are tracking electrical parameters in the PEO circuit [10; 11], electrical impedance spectroscopy of oxide layers [12], luminosity intensity tracking using high-speed photo-video recording [13; 14], photo-EMF recording [15], optical emission spectroscopy [16], infrared thermometry [17], coating thickness monitoring using various non-contact methods [18], acoustic signals (acoustic emission (AE) in the sound and ultrasonic ranges). The sound range is rarely used compared to the ultrasonic range, since it has a significantly lower noise immunity [19], therefore, in this paper, the authors consider AE only in the ultrasonic range.

AE tracking appears to be one of the most promising methods for PEO monitoring, since elastic waves accompany the process of stored energy relaxation with a rather wide range of known physical and chemical phenomena [20]. However, as far as we know, in the studies of AE during PEO, for a moment it was possible to identify only the primary correlation of the oxidation stages, with the integral characteristics of acoustic radiation without detailing the special aspects of the AE signals recorded on them. For example, in [21; 22], the authors discuss the relationship between acoustic radiation and PEO modes in the categories of "increase" and "decrease" of its level, even without specifying the parameters for estimating AE signals. In [23], using the AE threshold method, the correlation of AE signals with the stage of development of forming discharges (sparking, microarc, and arc discharges) was shown, and [24] described the correlation of the trends in the accumulation of counts during AE and the kinetics of the growth of oxide layers on the D16 alloy. In [25], the authors showed that with an increase in the oxide layer thickness, the acoustic signal shifts to a more low-frequency and high-amplitude region, which, in their opinion, indicates the localization and increase in the power of a single MAD. In [26], the acoustic emission monitoring of the PEO process, and the criterion assessment of the change in the AE amplitude, allowed improving the quality of the oxide layers, and its reproducibility on the D16AT alloy. In [27; 28], against the background of tracking the trends in AE energy changes, an attempt was made to separate acoustic signals into pulsed and continuous (resonant) types, with their following description by their parameters: amplitude, energy, rise time, and frequency at the peak. The work [29] presents the preliminary results of recording the AE signals obtained by PEO of AMg6 samples, and, in particular, establishes the synchronism of AE signal recording with the exposure cycle and shows the correlation of their temporal position with visual observations and literature data of optical measurements, using photo-video recording and photo-EMF analysis, as well as the PEO electrical parameters. However, identifying the PEO process stages by comparing their visual features with the AE amplitude features, gives a significant error in identifying the stage, and requires a more detailed understanding of the AE manifestation within the exposure cycle.

The analysis of indicated works showed that the parametric distributions of the used main parameters of the AE assessment significantly overlap (superimposed); therefore, the construction of diagnostic signs of PEO stages, using them has a high probability of error in identifying the type of emerging MADs. Consequently, to increase the AE method sensitivity, other approaches to the evaluation of acoustic signals are required.

The aim of the work is to identify the acoustic emission special features within the cycle of bipolar pulsed electrical action on the oxidized material (using the example of the AMg6 aluminum alloy) during plasma electrolytic oxidation as the basis for developing a new method for controlling PEO, to reduce the time for selecting its optimal mode through a more accurate detection of boundaries of various stages of the oxidation process.

METHODS

The subject of research is the AE that accompanies the formation of oxide layers on the AMg6 Al–Mg alloy (foreign analogue is alloy 1560, chemical composition, wt. %: 6.2 Mg; 0.65 Mn; 0.5 Ti; 0.4 Si; 0.3 Fe; 0.18 Zn; 0.087 Cu; Al – the base) at various modes of bipolar anode-cathode pulse action.

The samples for research had overall dimensions (140×20×6) mm^3, which were immersed in the electrolyte, not completely, in order to install the AE sensor directly on the sample. As a result, during PEO, only a part of the sample with the size of (60×20×6) mm^3 was oxidized. The rest, part of the sample, was insulated using an electrically insulating varnish and epoxy resin, which served as a contact medium and an AE sensor holder on the sample.

PEO was carried out on an innovative research self-made plant, produced by Togliatti State University consisting of a stainless steel bath with a volume of 15 l, an external cooling system based on a liquid/liquid heat exchanger, and a circulation pump for electrolyte thermostat control; pulse inverter power unit with a peak power of 40 kW, with a computer system to control the PEO modes for current and voltage in the specialized LabVIEW software. In the work, the bipolar (anode-cathode) pulsed mode of oxide layer formation was used as the most efficient, and promising in terms of obtaining the best quality, and properties

of oxide layers, which allows transferring the results of the AE analysis to the PEO anodic mode, without taking into account the cathode component.

The experimental constants for all PEO modes were the frequency of the forming current pulses – 500 Hz, i.e. the duration of the exposure cycle during PEO – 2 ms; the pulse duty cycle of the process current – 65 %; the ratio of the durations of the cathode and anode forming pulses is 55 %/45 %, respectively; pauses between the cathode and anode pulses – 50 %; electrolyte composition and temperature; PEO duration – 180 min.

During the experiment, the authors varied the root-mean-square current density j, A/dm^2 (6; 9; 12; 15 and 18 A/dm^2) through the sample, and the ratio of currents in the cathode and anode half-cycles C/A (0.70; 0.85; 1.00; 1.15 and 1.30), which were set at the PEO process initiation, and further kept constant by the plant control system. Totally, AE was recorded in 25 PEO modes, which almost completely cover the known and currently used modes of the oxide layer formation on aluminum alloys and, therefore, all PEO process stages (anodic passivation, anode sparking, anode-cathode MAO, and soft sparking modes [30]) and the MAD types (anode sparking, anode microarc and cathode microarc discharges, anode arc and cathode arc discharges, as well as discharges of A, B, and C types [31; 32]).

As an electrolyte, an aqueous solution based on KOH potassium hydroxide (3 g/l), $Na_4P_2O_7{\times}10H_2O$ sodium pyrophosphate (8 g/l), and $Na_2SiO_3{\times}5H_2O$ sodium metasilicate (12 g/l) was used. The electrolyte temperature during PEO was maintained by an external cooling system at a level of (285±3) K.

The AE was recorded directly from the sample, which determined the minimum coefficients of signal distortion and attenuation. Acoustic signals were converted into electrical ones, using the piezoeffect by a P111-(0.02-0.3) transducer (Russia) with a bandwidth of 20–800 kHz, with a main sensitivity in the frequency range up to 300 kHz. Further, the signals were amplified by a MSAE-FA010 two-stage broadband filter-amplifier (Russia), digitized, and recorded in frames with a duration of 40 ms (20 complete exposure cycles) every 1 min using an Advantech PCI-1714 12-bit A-to-D card (ADC) (Taiwan) at a sampling rate of 2 MHz, which provided the AE analysis frequency range up to 1 MHz. Therefore, in contrast to the works that used the threshold method of AE registration, the authors of this research excluded the omission in the record of AE changes, within the recorded exposure cycles. At the same time, the AE recording frame equal to the exposure cycle includes 4000 counts (4000 counts/2 MHz=2 ms). Synchronously with the acoustic signals, the same ADC recorded frames of voltage and current changes in the PEO cycles as well.

In our work [29], we described in detail the technical features and problems of obtaining an AE signal and protecting the sensor when an oxidized sample in an electrolyte.

The oxide layer thicknesses were measured, using a Konstanta K6 eddy-current thickness gauge (Russia), with a PD1 transducer, as well as on transverse metallographic sections using a Jeol JCM-6000 Neoscope II scanning electron microscope (Japan). The microhardness $HV_{0.1}$ was measured on cross sections in accordance with the GOST R 8.748-2011 standard on a Shimadzu DUH-211S dynamic microhardness tester (Japan). Wear resistance (linear wear rate) was evaluated using the ASTM G133 method on a Nanovea TRB-50N tribometer (USA). In more detail, the special aspects of measuring the thickness, hardness, and wear resistance of the obtained oxide layers using the specified techniques and the results obtained are described in [33; 34].

RESULTS

AE amplitude-time features during PEO

AE recording, together with visual tracking of the PEO process, showed that the main PEO stages have characteristics of AE signals that evolve synchronously with the observed MADs (Fig. 1). At the initial moment of time, the anode surface passivation, and the "barrier layer" formation occur as a result of chemical anodization and primary microarc breakdowns, which is accompanied by the onset and rapid increase in the AE amplitude (Fig. 1, stage I). As the barrier layer "strengthens", with the simultaneous oxide layer formation, the MADs amplify, begin to unite into cascades, and even change into separate (point) arc discharges at the stages II and III (Fig. 1), which is accompanied by AE signals of almost constant (Fig. 1, stage II) and increased (Fig. 1, stage III) amplitude. Then, for most of the studied modes, stage IV begins with a sharp drop in the AE signal amplitude, which coincides with the almost complete visual disappearance of burning MADs and the PEO process transition to the "soft sparking" mode.

In the process of comparing the sweep of the AE records and the time marks of stages I–IV (Fig. 1), obtained by visual observations of the change in the sample luminescence during PEO, the AE signs of the boundaries of the PEO stages were formed (Fig. 1). As standard visual boundaries of the PEO stages, the high-speed video recording freeze-frames given in [14], and similar to our experiment were taken. It is established that the first AE peak observed after the oxidation onset can be taken as the AE sign of the boundary of transition from stage I to stage II of PEO (Fig. 1, stage I). The beginning of the second AE peak equal to the first AE peak level or exceeding it (Fig. 1, stage II) can be taken as the sign of the boundary of the transition from stage II to stage III of PEO. The beginning of the recording section with a sharp drop in the AE amplitude (Fig. 1, stage III) can be taken as the AE sign of the boundary of the transition from stage III to stage IV of PEO. However, Fig. 1 shows that the amplitude "marks" and the PEO flow estimates have a time ambiguity and consequently, give an error during in situ monitoring of the process. In this regard, their use is unacceptable in the case when it is necessary to limit strictly the transition, from one stage to another, to achieve exactly the desired complex of functional properties of the layer.

Fig. 2 shows the results of the division of the studied PEO variants at the stage when using amplitude AE signs shown in Fig. 1.

Cyclic patterns of AE manifestation during PEO

If we synchronize the AE recording with the voltage change cycles, so that the beginning of the AE recording, frame coincides with the beginning of the anode PEO pulse half-cycle, and the length of the AE recording frame is equal to the full exposure cycle duration, then all the AE signals observed in various PEO modes can be divided into

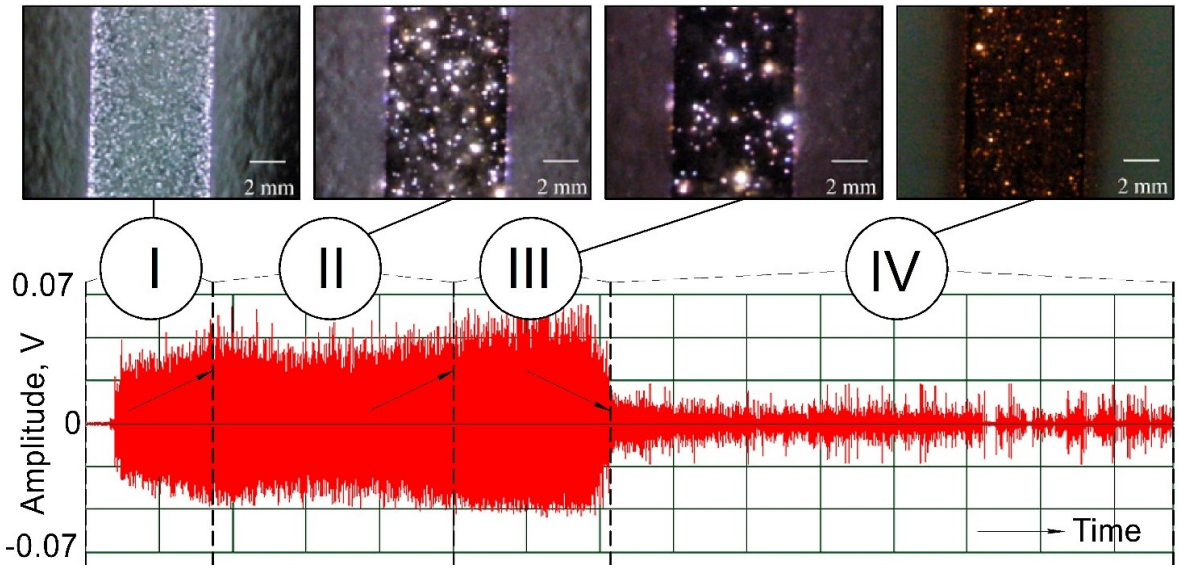

Fig. 1. *AE signs of PEO stages in the experiment and visual signs of microarc discharges on the sample during PEO under similar conditions [14]:*
I – anodic passivation and the beginning of sparking; II – PEO with the pronounced microarc discharges;
III – anode-cathode PEO stage; IV – "soft sparking" stage.
Record sweep duration along the OX (horizontal) axis – 180 minutes

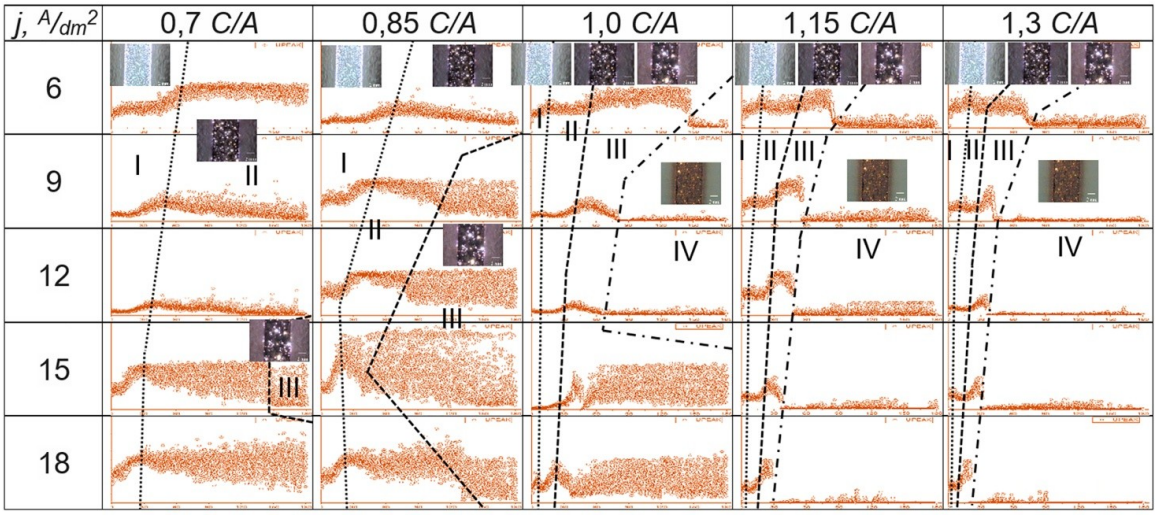

Fig. 2. *General nature of the change in the AE amplitude in 25 PEO modes, differing in current density j, A/dm^2 and the ratios of the positive to negative pulse currents C/A, at the oxidation duration of 180 minutes with a division into stages according to the visual and amplitude AE features shown in Fig. 1.*
The sizes of the axes on the graphs are fixed: along the OX (horizontal) axis – 180 minutes, along the OY (vertical) axis – 0.15 V

anode, anode-cathode, and cathode according to the location within the exposure cycle. At the same time, since the AE recording time is longer than the signal packet duration, all signals become pulsed (discrete) in form (Fig. 3). Signals of a continuous type were not observed within this approach to recording and analyzing the AE. We should note that the AE signals disappear both during the change of the forming pulse polarity and during the pulse itself (Fig. 3).

All peculiarities of the appearance of the signals recorded in the studied PEO modes can be reduced to the forms shown in Fig. 3.

We specially mention that in Fig. 3 b, the oscillations on the forming voltage curve *V(t)* (blue line) are associated with the power unit features and were not observed in the experiment, which is associated with the power unit design different from that used in [15].

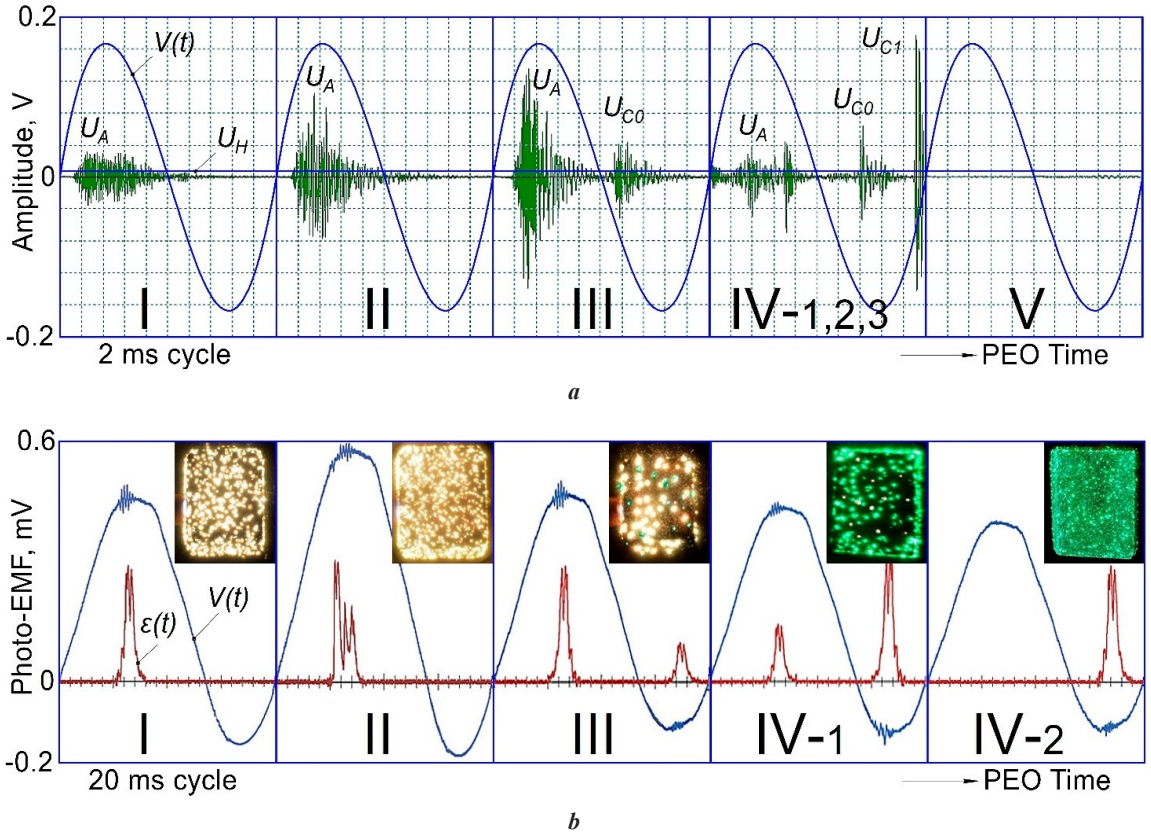

Fig. 3. *The main forms of AE signals observed at I–V PEO stages (**a**) and the comparison with the data [15] on recording photo-EMF ε(t) with video frames of PEO stages under similar conditions (**b**).*
I–V – PEO mode stages discovered by AE features;
U_A and U_{Ci} – the AE signal amplitude in the anode and cathode half cycles;
U_N – noise RMS value;
U_H or the black line – RMS value of AE signals at the beginning of PEO;
V(t) or the blue line – the voltage change curve showing the anode and cathode parts of the exposure cycle.
U_A, U_{Ci}, U_H and U_N are measured in V or dB of reference 1 mkV in accordance with Russian National Standard GOST 55045-2022. In the latter case, the same magnitudes are marked as L_{U_A}, $L_{U_{C_i}}$, L_{U_H} and L_{U_N}

At stage I of PEO, with visual signs of anodization, and the anode sparking onset (Fig. 1 and 2), in all the studied modes, the AE signals are recorded only in the anodic half-cycle (U_A) (Fig. 3 a). The AE signals are a burst of overlapping pulse signals, with approximately equal amplitude, dying out as the forming pulse amplitude voltage decreases (Fig. 3 a, I). The duration of the burst of AE signals of the PEO stage I, takes about 60 % of the half-cycle duration, and its beginning is shifted from the cycle beginning. The shift of the beginning, and the end of the AE signal burst from the boundaries of the anodic half-cycle, indicates the presence of the minimum voltage necessary to start the oxidation process. The gradual increase, and decrease in the amplitude at the beginning, and the end of the AE signal burst indicates a gradual increase/decrease in the scale of processes or its waviness, i.e., when several MAD "waves", or cascades, occur within one half-cycle.

AE signals of this type are summarized in Table 1 and, parametrically, in the amplitude-time domain for stage I, satisfy the condition (1) in this table. AE signs of the PEO stage I (depending on the mode) are observed up to oxide layer thicknesses of 0.4–14.0 μm, and then the process passes to stage II.

At stage II of PEO with clear visual signs of the occurrence of MADs distinguishing by greater brightness and intensity of movement along the anode compared to stage I, AE signals are also recorded only in the anodic half-cycle (U_A) (Fig. 3 a, II). In appearance, they are often close to the form of the PEO stage I signals, but have pronounced high-amplitude pulses (Fig. 3 a, II). In terms of the AE burst duration, the signals at the PEO stage II take from 60 to 100 % of the anodic half-cycle (half-period) duration, and their beginning is also shifted from the cycle beginning. In this case, high-amplitude AE pulses (emissions) are recorded in different parts of the AE signal burst. Parametrically, in the amplitude-time domain, the AE signals of the PEO stage II satisfy the condition (2) in Table 1.

At the PEO stage III (Fig. 3 a, III), the AE has detectable bursts of signals in the anode (U_A) and cathode (U_{C0}) half-periods of the exposure cycle, i.e., igniting MADs are recorded with the help of the AE in both half-periods. The main AE sign of this stage is that the total energy (power) of the signals in the anode half-cycle is higher than in the cathode one (Fig. 3 a, III), therefore, parametrically, in the amplitude-time domain, the AE signals of this type satisfy the condition (3) in Table 1. As well as in the anode

Table 1. *PEO stages and parametric conditions of AE signals in them*

PEO stage	AE type	Parametric conditions for the PEO stages identification in the AE amplitude-time area*	
I	I	$L_{U_H} > L_{U_N} + 3dB;\quad L_{U_A} < L_{U_H} + 6dB;\quad L_{U_{C0}}$ and $L_{U_{CI}} \le L_{U_N} + 3dB$	(1)
II	II	$L_{U_H} > L_{U_N} + 3dB;\quad L_{U_A} > L_{U_H} + 6dB;\quad L_{U_{C0}}$ and $L_{U_{CI}} \le L_{U_N} + 3dB$	(2)
III	III	$L_{U_A} > L_{U_N} + 3dB;\quad L_{U_{C0}} > L_{U_N} + 3dB;\quad L_{U_{C0}} < L_{U_A};\quad L_{U_{CI}} \le L_{U_N} + 3dB$	(3)
IV	IV-1	$L_{U_A} > L_{U_N} + 3dB;\quad L_{U_{C0}} > L_{U_N} + 3dB;\quad L_{U_{C0}} \ge L_{U_A};\quad L_{U_{CI}} \le L_{U_N} + 3dB$	(4)
	IV-2	$L_{U_A} \le L_{U_N} + 3dB;\quad L_{U_{C0}} > L_{U_N} + 3dB;\quad L_{U_{CI}} \le L_{U_N} + 3dB$	(5)
	IV-3	$L_{U_A} \le L_{U_N} + 3dB;\quad L_{U_{C0}} > L_{U_N} + 3dB$ or $L_{U_{C0}} \le L_{U_N} + 3dB;\quad L_{U_{CI}} > L_{U_N} + 3dB$	(6)
V	V	$L_{U_A} = L_{U_{C0}} = L_{U_{CI}} \le L_{U_N} + 3dB$	(7)

Note. L_{U_A}, $L_{U_{C0}}$ *and* $L_{U_{C1}}$, L_{U_H} *and* L_{U_N} *– the levels of* U_A, U_{C0} *and* U_{C1}, U_H *and* U_N *signals (Fig. 3), measured in dB relative to 1 mkV.*

part, in the cathode half-cycle, the AE signals (U_{C0}) do not have cyclic repeatability in time, and can occur in any part of the cathode half-cycle (pulse U_{C0} in Fig. 3). This behavior can be explained by the necessity of achieving a specified current in the cathode half-cycle, which cannot be ensured only by the process of electron flow, through the micropore channels into the sample. As a consequence, when a certain oxide layer thickness (about 20–50 μm) is reached, within the cathode half-cycle, the amplitude voltages reach 200–250 V, which is sufficient for the barrier layer breakdown, and leads to the MAD ignition with a concomitant sharp increase in the current [32]. AE signs of the PEO stage III, depending on the PEO mode in the experiment, begin to appear at coating thicknesses of 2.7–51.5 μm, which significantly refines the ignition moment of cathode MADs during aluminum alloy PEO relative to the data of [32].

The main difference of the PEO stage IV ("soft sparking" [14; 22]) from the previous ones is that the AE has the energy (power) of signals in the cathode half-cycle higher than in the anode one (Fig. 3 a, IV). Considering this general condition of type IV signals, the following subtypes were identified here: IV-1 – AE is recorded in the anode and cathode half-cycles and satisfies the condition (4) (Table 1); IV-2 – AE occurs only in the cathode half-cycle, i.e., the condition (5) is fulfilled (Table 1); IV-3 – type IV-2 AE signals are recorded, in which, except the U_{C0} cathode signals with the above described features, a U_{CI} signal is observed at the PEO stages III and IV (Fig. 3 a, IV). The physical nature of the U_{CI} signals is not yet fully understood, and requires additional research, but in time, they are always recorded at the end of the cathode half-cycle. Parametrically, in the amplitude-time domain, the type IV-3 AE signals satisfy the condition (6) (Table 1).

It is known [4; 32] that MADs in the cathode half-cycle occur at a coating thickness of more than 40–50 μm, which complies in the time of appearance of the stage IV AE signals, with our measurements of the coating thickness [29; 34], but only in the 0.7 C/A and 0.85 C/A modes at current densities of 9÷18 A/dm^2. In other modes (C/A=1.0; 1.15 and 1.3), where there is stage IV of PEO, the AE signals of this type begin to be recorded at coating thicknesses from 8.8÷36.9 μm, i.e., the stage of "soft sparking" begins to occur within them much earlier.

The PEO stage V was identified for the first time: it lacks acoustic signals distinguishing from background noise in the anode and cathode half-cycles (Fig. 3 a, V), so the condition for identifying this AE type takes the form of an expression (7) (Table 1). The PEO stage V was observed, as a rule, only in the modes with the highest current densities (12–18 A/dm^2) at C/A 1.15, and 1.30 and after observing the signs of stages I–IV, i.e., it falls on the end of the PEO process. Measurements showed that in the time interval of stage V, the layer thickness continues to increase at a low rate, and its properties change [34; 35], but visually at this stage, the MADs and their glowing on the sample are practically not recorded, and the AE signal, as noted above, does not exceed the noise one. Taken together, this does not allow speaking about full extinction of the PEO process.

Table 1 shows that under all conditions (1)–(7), the AE fold change is normalized relative to the levels L_{U_H} and L_{U_N}, which cannot be specified in absolute values. The latter

occurs, because these magnitudes depend on the sensitivity of the AE preformation used; the type and amount of contact medium; the place and accuracy of the AE transducer installation, and other factors affecting the transformation and attenuation of AE waves and ambient noise. In this regard, the values of L_{U_H} and L_{U_N} should be determined before PEO in a particular mode and taking into account the features of the AE equipment and PEO plant.

AE criterion for identifying the PEO process stage

One can conclude that, based on the identified patterns of AE manifestation during the pulse exposure period, the key features of dividing the forms of the AE cyclic manifestation into types are the time position of the signals (in the cathode and/or anode part), and the power (energy) correlation between them. Therefore, their tracking will allow identifying and classifying the stage of the PEO process implementation. For this purpose, the authors proposed a new "AE median" parameter-criterion – t_{AEm} (Fig. 4). AE median is a time mark in the exposure cycle, which divides the area under the curve, describing the nature of the AE measurement for the exposure cycle (S) into two equal parts ($S=S_1+S_2$, $S_1=S_2$, Fig. 4).

In this work, the *RMS(t)* curves were obtained from the AE recording frames (Fig. 1) using a sliding window equal to 10 counts (5 μs) with a shift step of 1 count.

Fig. 5 shows the results of dividing the AE recorded when accompanying the studied PEO modes, into the described stages using the above-defined signs of changing the AE shape and conditions (1)–(7) with the display of the proposed t_{AEm} parameter in the form of pictograms.

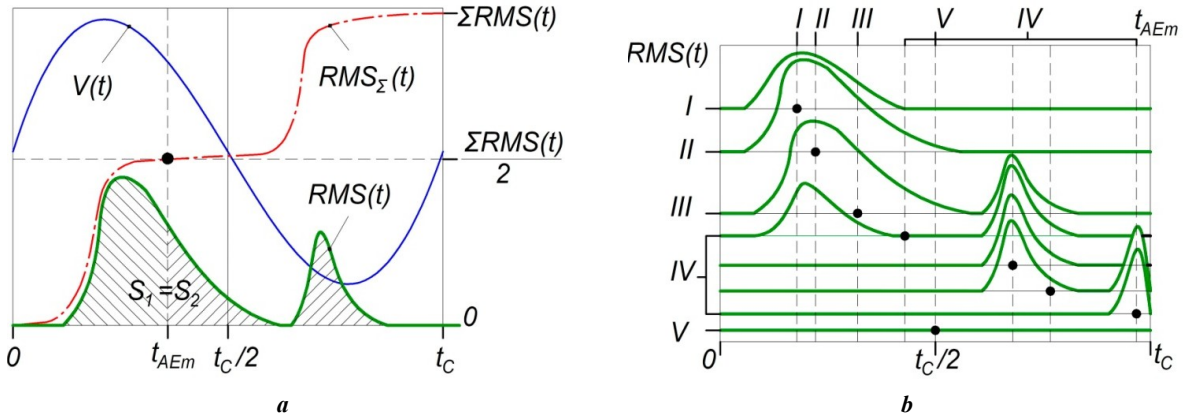

Fig. 4. *Explanatory diagrams for the method calculating of the t_{AEm} parameter-criterion (**a**) and the directions of its change when registering AE I–V waveforms indicated in Fig. 3 a (**b**)*

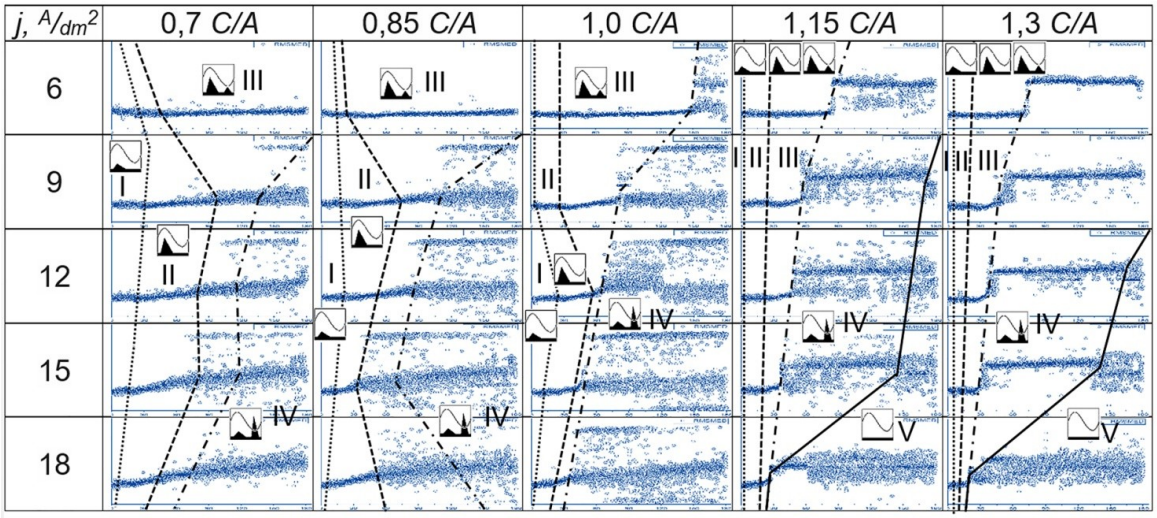

Fig. 5. *General nature of the change in the AE median in 25 PEO modes, differing in current density j, A/dm^2 the ratios of the positive to negative pulse currents C/A, at the oxidation duration of 180 minutes, divided into stages according to the conditions (1)–(7).*
The sizes of the axes on the graphs are fixed: along the OX axis – 180 minutes, along the OY axis – 4000 readings (eq. 2 ms).
The AE signal type observed at each stage is indicated by a pictogram corresponding to the type of signal in Fig. 4 b

DISCUSSION

The analysis of Fig. 2 and 5 shows that the PEO mode division into stages according to visual signs, and AE signal amplitude (Fig. 1 and 2) allows distinguishing stages I and II, but has a high inaccuracy at stages III and IV, and does not allow identifying stage V. The proposed "AE median" parameter t_{AEm} (Fig. 4 and 5), on the contrary, has a relatively low "sensitivity" to the PEO stages I and II, but allows identifying the presence of the cathode MADs in the AE record, which makes it possible to clearly identify the process stages III–V and detail stage IV into subtypes. Conditions (1)–(7) are universal, but their use requires preliminary studies and monitoring of several of the abovementioned amplitude parameters within their time marks of manifestation in each exposure cycle, which is not a trivial task.

Therefore, the calculation of the amplitude, and AE median for exposure cycles together allows describing the main features of all stages with just two numbers, and the identification of PEO stages in their two-parameter space seems to be the most promising for application towards PEO process monitoring. Moreover, since the errors of the proposed parameters, when detecting the PEO stages are of an antibate nature, their combined use should increase the probability of detecting the PEO stages. However, if we are talking only about the identification and monitoring of the PEO stages III–V, then the "AE median" parameter is self-sufficient.

Indeed, due to the developed parameter, it was possible to establish that the PEO modes, with the highest current density of 18 A/dm^2 at a current ratio *C/A* of 1.15 and 1.30 pass from stage III immediately to stage V (Fig. 5), which is accompanied by some increase in the thickness (Fig. 6 a), a decrease in the hardness (Fig. 6 b), an increase in the friction ratio in a pair, and a decrease in the wear resistance of oxide layers (Fig. 6 d). The PEO transition to stage V and an increase in its duration (Fig. 5) leads to a sharp increase in the friction ratio for the "oxide layer–steel ball" pair (Fig. 6 c), which is not entirely clear at this stage and requires additional research. One can also note, that as the duration of the PEO stage IV increases (Fig. 5), a decrease in the wear intensity of the friction pair is observed (Fig. 6 d), while the appearance of stage V, and an increase in its duration leads to an increase in the wear intensity of the pair in 1.5–2.5 times.

The joint analysis of Fig. 5 and 6 shows that the appearance of the cathodic MADs, close in power to anodic microarcs or exceeding them, and the PEO transition to the process stage IV lead to a slight decrease in the thickness of the formed oxide layers (Fig. 6 a), but at the same time, their average microhardness reaches the highest values

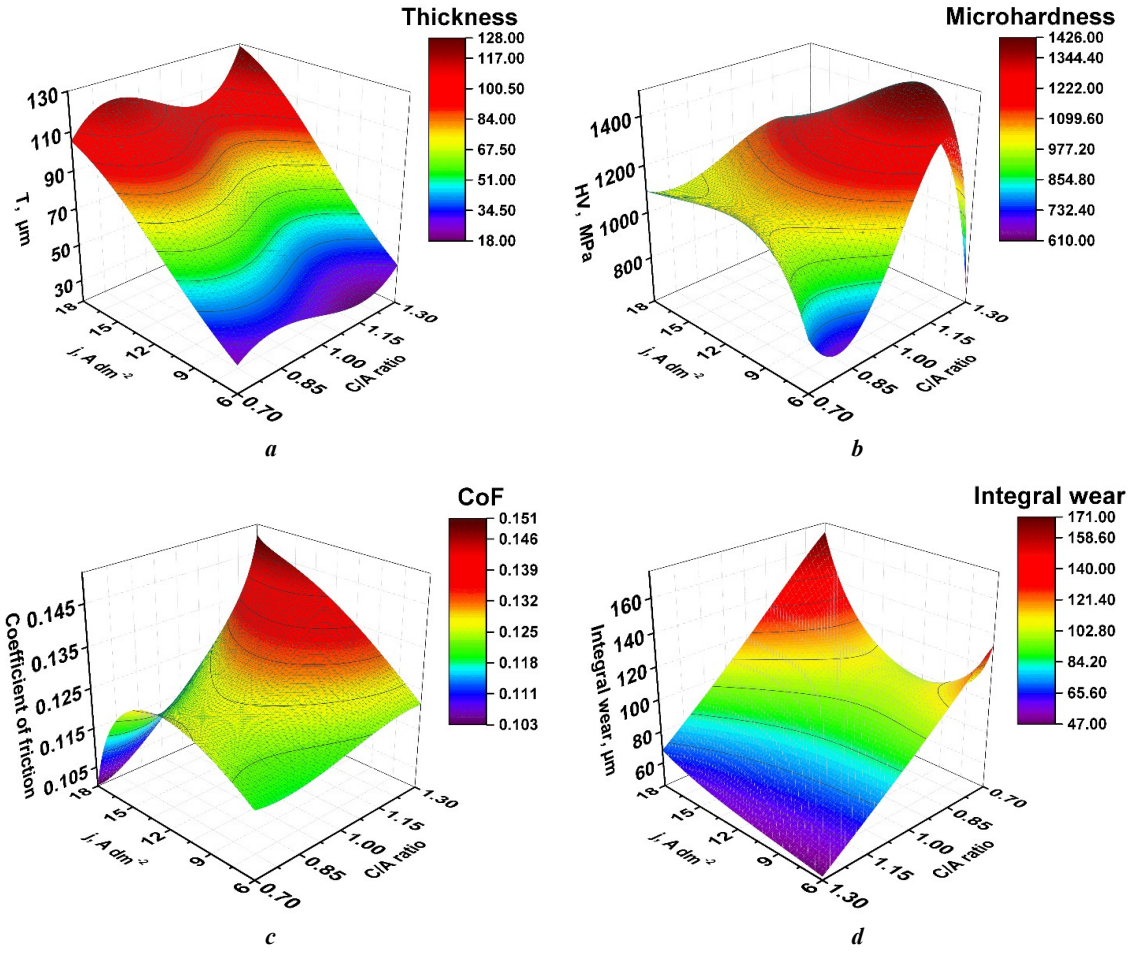

Fig. 6. *The dependences of the average thickness T, μm (**a**), microhardness HV 0.1, MPa (**b**), friction coefficient (**c**), and linear reduced wear (**d**) of the "oxide layer – steel ball" friction pair on the current parameters of the PEO mode*

(Fig. 6 b). Therefore, the introduced "AE median" parameter, which has an increased sensitivity to the PEO final stages, allows tracking their duration. Based on this, the transition to the oxidation process AE control is possible, by confirming reaching the specified stages in each PEO mode, and monitoring the compliance of the exposure time for each of them, which technologically should provide the required complex of coating properties. The latter is the subject for further experimental studies.

It should be noted that since the obtained data on the AE signal manifestation in the anode, and cathode half-cycles (half-periods) correlate with the light flashes during PEO [15] (Fig. 3 a and 3 b), the proposed parameter for dividing the PEO modes into stages will also be applicable when processing the results of observations during photo-video recording, and photo-EMF registration, where instead of changing the AE, for example, the glow intensity median in the anode and cathode exposure cycles can be monitored.

CONCLUSIONS

1. Possible forms of AE change within an exposure cycle during PEO of the AMg6 Al–Mg alloy in a bipolar pulse mode are established, which are reduced to five main types and three subtypes, as well as the boundaries (time points) of their change in a wide range of industrial PEO modes are identified. In this case, three subtypes of the AE change forms are of particular interest, since they refer to the "soft sparking" mode.

2. For the first time, a previously unknown stage V of the PEO process was identified, where a vapour-gas phase microarc breakdown to the metal substrate and the AE generated by it are practically missing.

3. The study shows that the approach to identifying the PEO stages using the standard "AE amplitude" parameter has a larger error, since it does not take into account the shape of the signals, and the half-period of their recording. The proposed new "acoustic-emission median" (AE median) parameter-criterion allows taking into account the indicated features, when dividing the PEO modes into stages according to AE, which makes it possible to specify the cyclic features of the AE manifestation determined in the work. It is experimentally shown, that the proposed parameter is efficient, has good accuracy and sensitivity to the subtypes of the AE signals, especially those recorded within the "soft sparking" mode.

REFERENCES

1. Mardare C.C., Hassel A.W. Review on the Versatility of Tungsten Oxide Coatings. *Physica Status Solidi A*, 2019, vol. 216, no. 12, article number 1900047. DOI: 10.1002/pssa.201900047.
2. Simchen F., Sieber M., Kopp A., Lampke T. Introduction to Plasma Electrolytic Oxidation–An Overview of the Process and Applications. *Coatings*, 2020, vol. 10, no. 7, article number 628. DOI: 10.3390/coatings10070628.
3. Martin J., Melhem A., Shchedrina I., Duchanoy T., Nominé A., Henrion G., Czerwiec T., Belmonte T. Effects of electrical parameters on plasma electrolytic oxidation of aluminium. *Surface and Coatings Technology*, 2013, vol. 221, pp. 70–76. DOI: 10.1016/j.surfcoat.2013.01.029.
4. Rogov A.B., Yerokhin A., Matthews A. The role of cathodic current in plasma electrolytic oxidation of aluminum: Phenomenological concepts of the "soft sparking" mode. *Langmuir*, 2017, vol. 33, no. 41, pp. 11059–11069. DOI: 10.1021/acs.langmuir.7b02284.
5. Rogov A.B., Matthews A., Yerokhin A. Relaxation Kinetics of Plasma Electrolytic Oxidation Coated Al Electrode: Insight into the Role of Negative Current. *The Journal of Physical Chemistry C*, 2020, vol. 124, no. 43, pp. 23784–23797. DOI: 10.1021/acs.jpcc.0c07714.
6. Rahmati M., Raeissi K., Toroghinejad M.R., Hakimizad A., Santamaria M. Effect of Pulse Current Mode on Microstructure, Composition and Corrosion Performance of the Coatings Produced by Plasma Electrolytic Oxidation on AZ31 Mg Alloy. *Coatings*, 2019, vol. 9, no. 10, article number 688. DOI: 10.3390/coatings9100688.
7. Butyagin P.I., Khokhryakov E.V., Mamaev A.I. Effect of Electrolyte Composition on the Wear Resistance of MAO Coatings. *Tekhnologiya metallov*, 2005, no. 1, pp. 36–40. EDN: KVFCPL.
8. Kuchmin I.B., Nechaev G.G., Soloveva N.D. Changes in the character of physical and chemical properties of two-silicate alkaline electrolyte for microarc oxidation over the production process. *Vestnik Saratovskogo gosudarstvennogo tekhnicheskogo universiteta*, 2013, vol. 4, no. 1, pp. 57–62. EDN: SEFXLX.
9. Hussein R.O., Northwood D.O., Nie X. Processing Microstructure Relationships in the Plasma Electrolytic Oxidation (PEO) Coating of a Magnesium Alloy. *Materials Sciences and Applications*, 2014, vol. 5, no. 3, pp. 124–139. DOI: 10.4236/msa.2014.53017.
10. Yerokhin A.L., Nie X., Leyland A., Matthews A., Dowey S.J. Plasma electrolysis for surface engineering. *Surface and Coatings Technology*, 1999, vol. 122, no. 2-3, pp. 73–93. DOI: 10.1016/S0257-8972(99)00441-7.
11. Suminov I.V., Belkin P.N., Epelfeld A.V., Lyudin V.B., Krit B.L., Borisov A.M. *Plazmenno-elektroliticheskoe modifitsirovanie poverkhnosti metallov i splavov* [Plasma-electrolytic surface modification of metals and alloys]. Moscow, Tekhnosfera Publ., 2011. Vol. 2, 512 p.
12. Golubkov P.E., Pecherskaya E.A., Kozlov G.V., Zinchenko T.O., Melnikov O.A., Shepeleva J.V. Application of impedance spectroscopy for research of the micro-arc oxidation process. *Proceedings – 2020 7th International Congress on Energy Fluxes and Radiation Effects (EFRE 2020)*. Tomsk, Publishing House of IAO SB RAS, 2020, pp. 773–777.
13. Arrabal R., Matykina E., Hashimoto T., Skeldon P., Thompson G.E. Characterization of AC PEO coatings on magnesium alloys. *Surface and Coatings Technology*, 2009, vol. 203, no. 16, pp. 2207–2220. DOI: 10.1016/j.surfcoat.2009.02.011.
14. Clyne T.W., Troughton S.Ch. A review of recent work on discharge characteristics during plasma electrolytic oxidation of various metals. *International Materials Reviews*, 2019, vol. 64, no. 3, pp. 127–162. DOI: 10.1080/09506608.2018.1466492.
15. Rakoch A.G., Gladkova A.A., Linn Z., Strekalina D.M. The evidence of cathodic micro-discharges during plasma electrolytic oxidation of light metallic alloys and micro-discharge intensity depending on pH of the electrolyte. *Surface and Coatings Technology*, 2015,

vol. 269, pp. 138–144. DOI: 10.1016/j.surfcoat.2015.02.026.
16. Wang L., Chen L., Yan Z., Fu W. Optical emission spectroscopy studies of discharge mechanism and plasma characteristics during plasma electrolytic oxidation of magnesium in different electrolytes. *Surface and Coatings Technology*, 2010, vol. 205, no. 6, pp. 1651–1658. DOI: 10.1016/j.surfcoat.2010.10.022.
17. Jin F.-Y., Wang K., Zhu M., Shen L.-R., Li J., Hong H.-H., Chu P.K. Infrared reflection by alumina films produced on aluminum alloy by plasma electrolytic oxidation. *Materials Chemistry and Physics*, 2009, vol. 114, no. 1, pp. 398–401. DOI: 10.1016/j.matchemphys.2008.09.060.
18. Golubkov P.E. Analysis of the applicability of thickness measurement methods dielectric layers in controlled synthesis protective coatings by micro-arc method oxygenating. *Izmerenie. Monitoring. Upravlenie. Kontrol*, 2020, no. 1, pp. 81–92. DOI: 10.21685/2307-5538-2020-1-11.
19. Rastegaeva I.I., Rastegaev I.A., Vikarchuk A.A., Merson D.L., Seleznev M.N., Vinogradov A.Yu. Acouctic emission-based feedback system for optimization of liquid processing in rotor devices. *Pribory i sistemy. Upravlenie, Kontrol, Diagnostika*, 2012, no. 5, pp. 25–31. EDN: SMJGQD.
20. Darband G.B., Aliofkhazraei M., Hamghalam P., Valizade N. Plasma electrolytic oxidation of magnesium and its alloys: Mechanism, properties and applications. *Journal of Magnesium and Alloys*, 2017, vol. 5, no. 1, pp. 74–132. DOI: 10.1016/j.jma.2017.02.004.
21. Tjiang F., Ye L., Huang Y.-J., Chou C.-C., Tsai D.-S. Effect of processing parameters on soft regime behavior of plasma electrolytic oxidation of magnesium. *Ceramics International*, 2017, vol. 43, no. 1, pp. S567–S572. DOI: 10.1016/j.ceramint.2017.05.179.
22. Tsai D.-S., Chou C.-C. Review of the Soft Sparking Issues in Plasma Electrolytic Oxidation. *Metals*, 2018, vol. 8, no. 2, article number 105. DOI: 10.3390/met8020105.
23. Bespalova Zh.I., Panenko I.N., Dubovskov V.V., Kozachenko P.N., Kudryavtsev Yu.D. Investigation of the formation of optical black oxide-ceramic coatings on the surface of aluminum alloy 1160. *Izvestiya vysshikh uchebnykh zavedeniy. Severo-Kavkazskiy region. Seriya: Estestvennye nauki*, 2012, no. 5, pp. 63–66. EDN: PFATGJ.
24. Mukaeva V.R., Gorbatkov M.V., Farrakhov R.G., Parfenov E.V. A study of the acoustic characteristics of plasma electrolytic oxidation of aluminum. *Elektrotekhnicheskie i informatsionnye kompleksy i sistemy*, 2018, vol. 14, no. 3, pp. 60–65. EDN: YSAZNZ.
25. Bao F., Bashkov O.V., Chzhan D., Lyuy L., Bashkova T.I. The study of the influence of micro-arc oxidation modes on the morphology and parameters of an oxide coating on the D16AT aluminum alloy. *Frontier Materials & Technologies*, 2023, no. 1, pp. 7–21. DOI: 10.18323/2782-4039-2023-1-7-21.
26. Boinet M., Verdier S., Maximovitch S., Dalard F. Plasma electrolytic oxidation of AM60 magnesium alloy: Monitoring by acoustic emission technique. Electrochemical properties of coatings. *Surface and Coatings Technology*, 2005, vol. 199, no. 2-3, pp. 141–149. DOI: 10.1016/j.surfcoat.2004.10.145.
27. Boinet M., Verdier S., Maximovitch S., Dalard F. Application of acoustic emission technique for in situ study of plasma anodizing. *NDT & E International*, 2004, vol. 37, no. 3, pp. 213–219. DOI: 10.1016/j.ndteint.2003.09.011.
28. Rastegaev I.A., Polunin A.V. Regularities and features of acoustic emission under plasma electrolytic oxidation of wrought Al-Mg alloy. *Journal of Physics: Conference Series*, 2021, vol. 2144, article number 012020. DOI: 10.1088/1742-6596/2144/1/012020.
29. Kaseem M., Fatimah S., Nashrah N., Ko Y.G. Recent progress in surface modification of metals coated by plasma electrolytic oxidation: Principle, structure, and performance. *Progress in Materials Science*, 2021, vol. 117, article number 100735. DOI: 10.1016/j.pmatsci.2020.100735.
30. Cheng Y.-L., Xue Z., Wang Q., Wu X.-Q., Matykina E., Skeldon P., Thompson G.E. New findings on properties of plasma electrolytic oxidation coatings from study of an Al–Cu–Li alloy. *Electrochimica Acta*, 2013, vol. 107, pp. 358–378. DOI: 10.1016/j.electacta.2013.06.022.
31. Troughton S.C., Clyne T.W. Cathodic discharges during high frequency plasma electrolytic oxidation. *Surface and Coatings Technology*, 2018, vol. 352, pp. 591–599. DOI: 10.1016/j.surfcoat.2018.08.049.
32. Polunin A.V., Denisova A.G., Cheretaeva A.O., Shafeev M.R., Borgardt E.D., Rastegaev I.A., Katsman A.V. The effect of process current parameters on the properties of oxide layers under plasma electrolytic oxidation of AMg6 alloy. *Journal of Physics: Conference Series*, 2021, vol. 2144, article number 012018. DOI: 10.1088/1742-6596/2144/1/012018.
33. Polunin A.V., Cheretaeva A.O., Shafeev M.R., Denisova A.G., Borgardt E.D., Rastegaev I.A., Katsman A.V., Krishtal M.M. Mechanical and anticorrosive properties of oxide layers formed by PEO on wrought 1560 Al-Mg alloy: The effect of electric current parameters. *AIP Conference Proceedings*, 2022, vol. 2533, article number 020029. DOI: 10.1063/5.0098844.